https://doi.org/10.5194/nhess-2019-179
Preprint. Discussion started: 11 June 2019

Natural Hazards and Earth System Sciences
Discussions

Infrasound and seismoacoustic signatures of the September 28th 2018 Sulawesi super shear earthquake

Christoph Pilger[1], Peter Gaebler[1], Lars Ceranna[1], Alexis Le Pichon[2], Julien Vergoz[2], Anna Perttu[3], Dorianne Tailpied[3], Benoit Taisne[3]

1 – BGR (Federal Institute for Geosciences and Natural Resources), Hannover, Germany
2 – CEA, DAM, DIF (Commisariat à l'Energie Atomique et aux Energies Alternatives), Arpajon, France
3 – EOS / NTU (Earth Observatory of Singapore / Nanyang Technological University), Singapore

Corresponding author: Christoph Pilger; BGR, Hannover, Germany; christoph.pilger@bgr.de

Abstract

A magnitude 7.5 earthquake occurred on September 28th 2018 at 10:02:43 UTC near the city of Palu on the Indonesian island of Sulawesi. It was a shallow, strike-slip earthquake with fractures up to the surface and a rupture length of about 150 km. Moreover, this earthquake was identified as one of very few events having a super shear rupture speed.

Clear and long-lasting infrasound signatures related to this event were observed by four infrasound arrays of the International Monitoring System of the Comprehensive Nuclear-Test-Ban Treaty Organization as well as one national infrasound station in Singapore. Although these infrasound stations SING (Singapore), I39PW (Palau), I07AU (Australia), I40PG (Papua New Guinea) and I30JP (Japan) are located in large distances between 1800 km and 4500 km from the earthquake's epicentral region, the observed infrasound signals associated to this event were intense, including both seismic and acoustic arrivals. The seismic-to-acoustic coupling at nearby terrain features is supposed to generate distinct infrasonic signatures clearly recordable at remote infrasound arrays.

A detailed study of the event-related observations and the potential infrasound generation mechanisms is presented covering range- and time-dependent infrasound attenuation and propagation modeling, characterization of the atmospheric background conditions as well as identification of the regions of seismoacoustic activity by applying a backtracking method from the infrasound receivers to potential source regions. The back-projection of infrasonic arrivals allows to estimate that the main infrasound source region for the Sulawesi earthquake is related to the extended rupture zone and the nearby topography. This estimation and the comparison to other super shear as well as large regional earthquakes identifies no clear connection between the earthquake's super shear nature and the strong infrasound emission.

Keywords

Infrasound; seismoacoustics; attenuation; propagation modeling; Sulawesi; super shear; earthquake

Natural Hazards and Earth System Sciences
Discussions

1. Introduction

Indonesia is located in a region with a very high natural seismicity above a complex setting of plate tectonics. Subduction zones of convergent plate boundaries in this region define the largest faults of the Earth's crust, and the region of highest and most intense earthquake activity. In fact, some of the strongest and most destructive earthquakes recorded during the last decades have occurred in Indonesia, like the 2004 moment magnitude (Mw) 9.3 Sumatra-Andaman earthquake and various other events with Mw larger than 8 (*Pailoplee, 2017*). These strong offshore events can often generate large and devastating tsunamis. Additional crustal scale faults are also located on the Indonesian island of Sulawesi, including the Palu-Koro fault transecting the Northern part of the island (*Katili, 1978*). Frequent seismic activity is associated to this fault, resulting in at least 60 earthquakes larger than magnitude 5 within the last 20 years and four events larger magnitude 6 previous to the event discussed in this study.

The September 28th 2018 Sulawesi earthquake occurred at 10:02:43 UTC near the Indonesian city of Palu on the island of Sulawesi. It was estimated by the United States Geological Survey (USGS) as a Mw 7.5 strike slip earthquake along the Palu-Koru fault with a hypocenter location of 0.256°S and 119.846°E and a depth of about 20 km. Modeling indicates that the majority of the slip occurred shallow on the fault (above 10 km) with an offset of up to 7 m horizontal slip and a dip slip of up to only 2 m (*Socquet et al., 2019*). The rupture zone of the event extended north-to-south over roughly 150 km, along the fault and through the city of Palu, with a high rupture velocity of 4.1 km/s in average, thus indicating it to be a so called super shear event having rupture velocities higher than the corresponding shear velocities (see *Bao et al., 2019; Socquet et al., 2019*). The earthquake resulted not only in intense ground shaking up to "considerable damages" of Modified Mercalli Intensity IX, but also in liquefaction, landslides, and local tsunamis within Palu bay (see *Heidarzadeh et al., 2019; Omira et al., 2019*). A large number of precursory earthquakes as well as aftershocks happened in the course of this event.

The intense ground shaking of either the epicentral region or the nearby topography from the Sulawesi earthquake resulted in strong and clearly observed infrasound signatures, which are the focus of this study. Infrasound, which is the sub-audible part of acoustic waves below 20 Hz, is generated by a large number of natural and anthropogenic sources (e.g. see *Le Pichon et al., 2010, 2019*) and can propagate over distances of thousands of kilometers with little attenuation to highly sensitive infrasound arrays. Many sources of either explosive or eruptive characteristic, or those coming along with large mass movements can generate infrasound (e.g. *Gibbons et al., 2015a; Pilger et al., 2018*), including earthquakes.

Reports on infrasound from earthquakes in the USA (*Mutschlecner and Whitaker, 2005*) as well as in Peru, China and Chile (*Le Pichon et al., 2002, 2003, 2006*) indicate that the epicentral ground movement generates infrasonic pressure waves. Further studies on the Mw 9.3 Sumatra-Andaman earthquake (*Le Pichon et al., 2005)* and on Italian earthquakes (*Marchetti et al., 2016; Shani-Kadmiel et al., 2017; Hernandez et al., 2018)* also highlight infrasound generated from secondary phenomena like remote ground motion of mountain chains or extended basin areas, and from tsunami waves hitting the coastline. This secondary infrasound is often called seismoacoustic waves, since the seismic waves (longitudinal, shear or surface) generated by an earthquake propagate to distant terrain features where the wave energy is partly converted to atmospheric acoustic waves in the infrasound frequency range (e.g., see *Arrowsmith et al., 2010; Hedlin et al., 2012*).

Although there is quite a large number of studies about infrasound generated by earthquakes, only a small number of earthquakes with a super shear rupture speed have been identified within the last 20 years (e.g. Izmit/Turkey in 1999, see *Bouchon et al., 2000*; Kunlunshan/Tibet in 2001, see *Bouchon and*

https://doi.org/10.5194/nhess-2019-179
Preprint. Discussion started: 11 June 2019

Natural Hazards and Earth System Sciences
Open Access
Discussions

Vallee, 2003; Denali/Alaska in 2002, see *Dunham and Archuleta, 2004;* Quinghai/China in 2010, see *Wang and Mori, 2012*; Craig/Alaska in 2013, see *Yue et al., 2013*), and only one publication known to the authors identifies and investigates infrasound observations of a super shear earthquake, namely the Denali 2002 earthquake (*Olson et al, 2003*). Therefore, one of the main tasks of this paper is to investigate the potential of a connection between super shear earthquakes and infrasound recordings of large amplitude.

This paper is structured as follows: Section 2 describes the data and methods applied within this study; section 3 highlights the observations of infrasound and seismoacoustic signatures at remote infrasound arrays; section 4 describes the modeling of infrasound attenuation and propagation and compares it to the observations; section 5 provides a back-tracking approach to identify the acoustic source regions of the observed signals and discusses the event in comparison with similar earthquakes.

2. Data and Methods

Data from various infrasound arrays of the International Monitoring System (IMS) established under the Comprehensive Nuclear-Test-Ban Treaty (CTBT), are used within this study. Figure 1 shows the earthquake epicenter as well as the nearest stations around the event.

The two IMS infrasound stations closest to the earthquake epicenter clearly registered the event (I39PW in Palau and I07AU in Northern Australia). Two further IMS stations at larger distances found clear indications of signals related to the earthquake (I40PG in Papua New Guinea and I30JP in Japan). However, two other Australian stations (I04AU and I06AU) as well as all of the more distant IMS infrasound arrays recorded no signals related to the earthquake source.

Additional data from a single infrasound sensor in Singapore (SING) was investigated and also showed signatures related to the earthquake. However, due to a lack of array calculations and directional information by only a single sensor, no further studies are applied for this data.

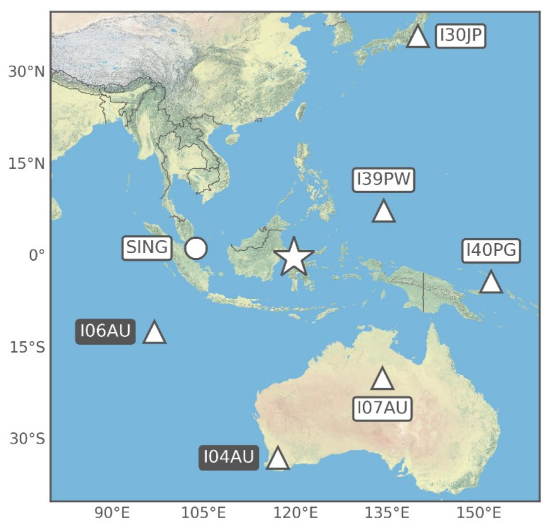

Fig 1: Map of the Sulawesi earthquake epicenter (asterisk) and the locations of the nearest surrounding infrasound stations (the circle corresponds to a single-sensor station, the triangles to multi-sensor IMS arrays; white-labeled stations registered the event, black-labeled ones did not).

https://doi.org/10.5194/nhess-2019-179
Preprint. Discussion started: 11 June 2019

The PMCC method (Progressive Multi-Channel Correlation, see *Cansi, 1995*; available from the DTK-GPMCC application in the NDC-in-a-box package) is applied to the raw differential pressure recordings at each of the IMS infrasound arrays' microbarometers to derive advanced data parameters like back-azimuth, apparent velocity and frequency content of coherent signals thereby associated to different events (see figure 2). Signals are identified as pixel information in distinct time steps and frequency bands and are clustered to signal families related to the same event. 1/3 octave band configurations with an inverse frequency distributed window length are implemented between 0.01 and 4.4 Hz (*Garces, 2013*). Signals can be associated to a certain source by e.g. applying cross bearing techniques on the back-azimuth directions of two or more arrays. The seismic or acoustic origin as well as the propagation of signals can be identified by the apparent velocity and frequency content of the recordings.

In order to further investigate and understand the infrasound detection pattern in the region following the Sulawesi earthquake, various simulations were performed to compute acoustic attenuation and to simulate infrasound propagation between the source and the stations. Infrasound attenuation (see figure 3) was calculated using a frequency-dependent, semi-empirical modeling technique coupled with realistic atmospheric specifications along the infrasound propagation path (*Le Pichon et al., 2012; Tailpied et al., 2017*) in order to draw a range- and frequency-dependent attenuation map estimating the acoustic pressure loss between source and receivers in decibel (dB). The attenuation of the signal at each station is associated to a confidence index that integrates uncertainties from the propagation modeling and the atmospheric specifications. Infrasound propagation (see figure 4) was modeled using a two-dimensional Parabolic Equation method (NCPA PAPE, see *Waxler et al., 2017*) to quantify the ducting and amplitude decrease between source and receivers.

In both attenuation and propagation modeling, data from the European Centre for Medium-range Weather Forecast (ECMWF) meteorological model are used to derive the effective sound speed as the most important background parameter for infrasound propagation. Indeed, this parameter, defined as adiabatic sound speed modified by horizontal winds in the propagation direction of the modeled sound, is used to provide the atmospheric background conditions along the propagation path between the source and the stations (*Wilson, 2003*). Ducting along tropospheric, stratospheric or thermospheric waveguides (*Drob et al., 2003*) can be estimated in the same manner as the total amplitude loss from geometric spreading as well as atmospheric attenuation (*Sutherland and Bass, 2004*). ECMWF values are used from 0 to 60 km altitude and merged with temperature and wind climatologies above (MSISE00 and HWM07, see *Picone et al., 2002, Drob et al., 2008*) to provide seamless effective sound speed profiles from 0 to 140 km altitude.

Backtracking of the coherent earthquake-related signals observed at infrasound arrays to their source region is performed within this study using a seismoacoustic method similar to that of *Marchetti et al. (2016)* or *Shani-Kadmiel et al. (2017)*, which is also part of the built-in capabilities of PMCC (see figure 5). Assumed is a conversion of the initial seismic wave with crustal propagation velocities of e.g. 4 km/s to acoustic waves with average celerities of e.g. 0.3 km/s at certain terrain features, like steep or flat topography as e.g. mountain chains, islands, cliffs or extended plains. This method identifies the seismoacoustic conversion areas and thus infrasonic source regions for the signals observed, taking into account for each PMCC pixel the arrival time and back-azimuth direction relative to a point source in space and time, here the Mw 7.5 earthquake epicenter. The cumulative sum and frequency of occurrence of the backtracked origin locations therefore allows to identify seismoacoustic source regions, either of epicentral or secondary origin.

https://doi.org/10.5194/nhess-2019-179
Preprint. Discussion started: 11 June 2019

Natural Hazards and Earth System Sciences
Open Access
Discussions

3. Observations

The September 28th 2018 Sulawesi earthquake was identified in the recordings of four IMS infrasound arrays: I39PW, I07AU, I40PG and I30JP. Four to six hours of differential pressure recordings from these stations following the earthquake origin time (10:02:43 UTC) are analyzed using the PMCC method described in section 2. Signal parameters related to the earthquake are extracted from the PMCC results in terms of arrival time and duration as well as direction of origin and apparent signal velocity.

Table 1 summarizes these observed parameters for the four IMS arrays and for the earthquake-related signal also identified in SING station data. Furthermore, source-to-station distances as well as expected back-azimuth directions and arrival times using a celerity (speed over ground) of 300 m/s are presented for comparison. Figure 2 provides a graphical representation of the main findings for the four IMS stations, highlighting epicentral infrasound arrivals and their acoustic characteristics in the observations but also seismoacoustic and seismic signatures related to the event.

Table 1: Findings from the observations of five infrasound stations and from theoretical distance-azimuth calculations to the Sulawesi epicenter. Main signals are labeled with "IS" (infrasound), secondary signals are labeled "SA" (seismoacoustic).

Station	**SING**	**I39PW**	**I07AU**	**I40PG**	**I30JP**
Distance to epicenter (km)	1788	1845	2689	3604	4474
Expected back-azimuth (°)	94	243	322	276	213
Expected 300 m/s arrival time (UTC)	11:42	11:45	12:32	13:23	14:11
Observed arrival time (UTC)	IS) 11:50	IS) 11:36 SA) 12:34	IS) 12:08 SA) 11:22	IS) 13:05 SA) 12:37	IS) 14:30
Observed signal duration (min)	IS) 10	IS) 25 SA) 7	IS) 44 SA) 16	IS) 24 SA) 8	IS) 33
Observed mean celerity (m/s)	IS) 267	IS) 290 SA) 200	IS) 304 SA) 514	IS) 309 SA) 380	IS) 263
Observed mean back-azimuth (°)	- (no array)	IS) 251 SA) 257	IS) 319 SA) 321	IS) 275 SA) 276	IS) 209
Observed mean apparent velocity (m/s)	- (no array)	IS) 383 SA) 359	IS) 356 SA) 371	IS) 351 SA) 360	IS) 436

https://doi.org/10.5194/nhess-2019-179
Preprint. Discussion started: 11 June 2019

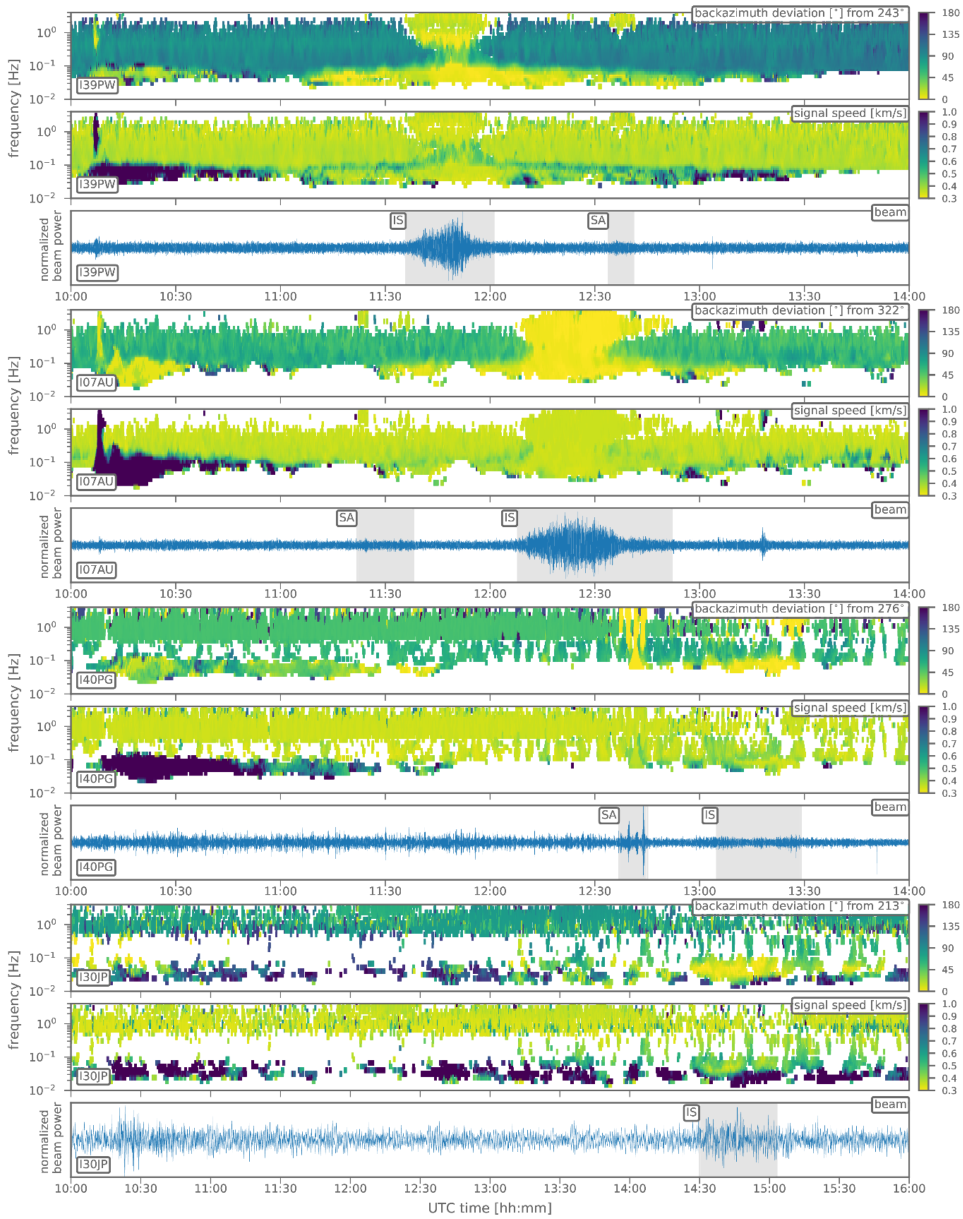

Fig 2: Waveform beams and PMCC-derived results for the four infrasound arrays I39PW, I07AU, I40PG and I30JP (stations are sorted by distance from above, three frames per station, station labels in the lower left corners). Shown in the corresponding stations' top frames are the observed back-azimuth deviations from the direction to the earthquake epicenter (see labels in the upper right corners), in the middle frame the observed apparent velocities, and in the bottom frame the waveform beams. The whole 360° back-azimuth observations are converted to the given deviation plotting of ± 180°. Apparent velocities are saturated above 1 km/s. Beams are bandpass-filtered between 0.6 - 4 Hz and four hours of data are shown with the exception of I30JP where the beam is bandpass filtered between 0.02 - 0.1 Hz and six hours of data are shown.

https://doi.org/10.5194/nhess-2019-179
Preprint. Discussion started: 11 June 2019

The main findings of the infrasound observations and PMCC analyses related to the earthquake are:

- Initial seismic waves with high-frequency components (0.3-3 Hz) are found in I39PW and I07AU data arriving four to six minutes after the origin time, indicating apparent P-wave velocities of 4-10 km/s, lasting about two minutes. These are followed by low-frequency (0.05-0.5 Hz), quasi-continuous seismic waves observed in all four arrays, likely related to seismic shear and surface waves, having velocities of 1-3 km/s. Aftershock activity as well as seismic signals from other regional earthquakes are also present in figure 2 for the hours after the main earthquake; aftershocks include 12 events of magnitude 5 or greater, and 40 events of magnitude 4 or greater within six hours following the event (source: USGS). Values for the arrival of seismic waves are not integrated in table 1, since the local infrasound observations generated from ground-shaking of the sensors are not the focus of this study. Nevertheless, the infrasound sensors do work fairly well as seismic arrays here (e.g. see *Gibbons et al., 2015b*) and the earthquake related seismic arrivals can clearly be identified in figure 2 having apparent velocities exceeding 1 km/s (drawn with dark blue colors in the middle frame plot of each station indicating seismic and not acoustic signal speeds).

- Epicentral infrasound is clearly observed and produces the main signal with the largest waveform amplitudes in I39PW and I07AU (beams are plotted in figure 2 in the bottom frame plots of the respective stations, signals are highlighted by grey rectangles and “IS” labels). The analysis shows a broadband-frequency content (0.05 to 4.4 Hz) and long signal durations of 25 and 44 minutes. Figure 2 emphasizes these signals since the back-azimuth calculations as well as the beamforming are focused on the respective theoretical back-azimuth for the epicenter calculated for each station (yellow colors in the azimuth frame of each station indicating low to zero back-azimuth deviations from this value). The low deviations from the theoretical back-azimuth directions (3° and 8°, see table 1 for the corresponding values) confirm the signals to be associated to either the epicenter, the rupture process at the surface or the ground shaking of topographic features on the island of Sulawesi. An azimuthal sweep is observed in the I07AU data from south to north (directions of 316° to 323°), consistent with the north-to-south rupture along 150 km. The other three stations only show weak or no such sweeps.

- For the more distant stations I40PG and I30JP, the epicentral infrasound is consistent with the theoretical back-azimuths (1° and 4° deviation), but mostly allocated with frequencies below 0.1 Hz, indicating larger absorption of the high-frequencies along the long-distance propagation (see section 4 for the corresponding propagation modeling). The high-frequency pulses in the I40PG recordings around 12:40 UTC are associated to a secondary signal, which is discussed in the end of this section.

- In general, the observed back-azimuths fit very well to the theoretical ones calculated for the epicenter for all four stations, allowing the application of a cumulative back-tracking method to locate the source regions of the observed infrasonic signals in section 5. The epicentral signals’ mean apparent velocities are all in the acoustic range valid for stratospheric propagation (350 to 380 m/s, see table 1), with the exception of I30JP having higher mean apparent velocities of 436 m/s. This together with low celerity values of 263 m/s and appearance of only low-frequency signals at this station strongly indicates thermospheric propagation for I30JP instead of stratospheric. Thermospheric arrivals are expected to also be present in the other stations’ observations apart from the dominant stratospheric ones; their later arrival time and lack of high-frequency content correspond to the long-lasting signal families following the main signal peak for many minutes in the low frequencies. These signal families can be observed together with low-frequency seismic wave activity and low frequency acoustic components from the stratospheric ducting, discernible only to a certain degree by the apparent velocities and arrival times. The celerities observed at I39PW, I07AU and I40PG as well as the observed arrival times and signal durations well correspond to the expected arrival times calculated

https://doi.org/10.5194/nhess-2019-179
Preprint. Discussion started: 11 June 2019

using a 300 m/s celerity of average stratospheric propagation, quite close to the actually observed values at I39PW, I07AU and I40PG (see table 1). The expected arrival times for these stations are clearly within the main signals' observed time window and are only 2 to 6 minutes shifted from the respective mid-point of the observed arrivals' time window (arrival time plus half of the signal duration).

- Microbaroms are also present in the recordings of I39PW and I07AU around 0.2 Hz and dominant before and after the earthquake signals, as well as surf or potentially anthropogenic noise in I40PG and I30JP data around 1 Hz during the complete observation. These background (noise) signals can clearly be separated, by back-azimuths (greenish colors in the top frame plots) from the epicentral signal. Infrasound signals can generally be distinguished from the seismic arrivals by their signal speed.

- Secondary signals are identified in I07AU, I39PW and I40PG data, coming from nearly epicentral directions and having acoustic velocities. They have high frequency content (above 1 Hz) and celerities below 200 or above 380 m/s, thus excluding purely acoustic waves e.g. traveling through thermosphere or troposphere. These arrivals could be seismoacoustic precursors and successors related to the earthquake (their signal parameters are provided in table 1 and highlighted in figure 2 with the label "SA"). A conversion of seismic to acoustic waves at certain, distinct terrain features might be responsible for this kind of signals. Islands between Java and East Timor (south of Sulawesi) could be the rough source region of the I07AU and I39PW signals, while islands of North Maluku (east of Sulawesi) may be the source of the seismoacoustic signals in I40PG. Further details on back-tracking and thus identifying acoustic source regions are provided in section 5. Nevertheless, from the given observations it is not possible to certainly confirm these secondary signal locations as seismoacoustic source regions. None of the secondary signatures are observed at more than one station and smaller groups of signals come from all regions around Sulawesi, also including neighboring islands like Borneo. These signals are not necessarily associated to the earthquake, and could be due to uncertainties in the array processing or back-tracking methods, or they are associated to other local infrasound or other noise sources and are just coincidental to the earthquake in direction and timing.

4. Modeling Results

Attenuation and propagation modeling are performed in this section to confirm and interpret the observed epicentral infrasound signatures as described above. Attenuation modeling is used to estimate the frequency-dependent transmission loss of a signal reaching the different infrasound stations, thereby characterizing its detectability. Propagation modeling is necessary to identify observed and expected signal arrivals and associate them to the prevailing atmospheric conditions between source and receivers and the corresponding ducting behavior.

Figure 3 shows the quantification of infrasonic transmission loss from atmospheric attenuation calculations (see *Tailpied et al., 2017*) as well as a representation of the stratospheric wind field in terms of intensity and directionality. Simulations are performed within an 80° x 80° area around the earthquake epicenter for source frequencies of 0.2 Hz and 3 Hz. At the low frequency of 0.2 Hz (figure 3a), where most of the acoustic energy is concentrated following calculations with the INFERNO software (see *Garces, 2013*), the attenuation at all nearby infrasound stations is quite similar: values in the map and their uncertainties are 66.8 ± 4.4 dB for I07AU, 67.3 ± 4.4 dB for I39PW, 69.0 ± 4.3 dB for I40PG and 69.3 ± 4.3 dB for SING. While values at these four stations indicate a northwest-to-southeast corridor of signal amplitudes in the same order of magnitude, the other stations in northeastern and southwestern directions have slightly higher attenuation values of 73.7 ± 4.2 dB for I06AU, 77.3 ± 3.8 for I04AU and 78.2 ± 4.0 for I30JP, indicating less favorable ducting conditions and detection probabilities at these stations.

https://doi.org/10.5194/nhess-2019-179
Preprint. Discussion started: 11 June 2019

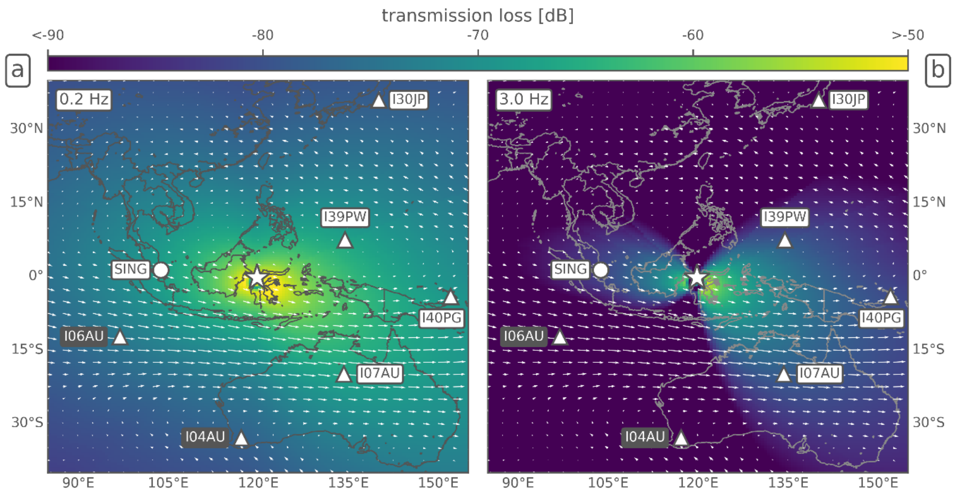

Fig 3: Attenuation map quantifying the acoustic pressure loss in dB (color-coded), calculated for (a) 0.2 Hz and (b) 3 Hz source frequencies on a 0.5° x 0.5° grid. Arrows show direction and intensity of the stratospheric wind field averaged between 30 and 60 km for the 28th of September 2018. The largest arrows represent a value of 25 m/s. For figure symbols and station labels see figure 1.

The similarity of the attenuation values is consistent with the fact that low frequency signals are less affected by propagation effects along the path. Drawing the same picture with a source frequency of 3 Hz (figure 3b) indicates a different situation: station values now are 78.3 ± 17.9 dB for I07AU, 79.7 ± 21.4 dB for I39PW, 81.0 ± 13.7 dB for I40PG and 84.1 ± 24.2 dB for SING. Those values are still quite similar along the abovementioned corridor, although the uncertainties for the calculation are increased. The attenuation calculated from the epicentral source into all directions to a stronger degree visualizes for the high frequencies a focal effect in eastern and western directions with better observation conditions, while having increased attenuation regions and thus more unfavorable detection conditions in northern and southern directions. The other stations' values in these directions are 101.4 ± 26.6 dB for I06AU, 118.7 ± 34.9 for I04AU and 107.0 ± 32.1 for I30JP, indicating remarkably higher attenuation for these three stations due to propagation effects and atmospheric conditions and explaining, why no high-frequency signals (or signals at all) are observed at the respective stations.

Stratospheric wind conditions affect the propagation especially for the higher frequencies and point out the general possibility and effectiveness of a stratospheric duct. This is consistent with the fact that high frequency signals are more sensitive to the atmospheric conditions along the propagation path, also explaining the higher uncertainties in the calculation of these values. The stratospheric wind fields shown in figure 3 support this sensitivity by estimating the direction of the dominant stratospheric wind regime, which is eastward on the southern hemisphere's low latitudes, and the intensity of this 30 to 60 km average, which is up to values of 25 m/s. Strong tailwinds thus support the stratospheric propagation to I07AU, while strong head- and crosswinds hamper it towards I04AU and I06AU. Winds are weaker from the source towards the other stations, mostly due to the equatorial wind situation of zonal stratospheric winds changing their direction here, rendering possible the simultaneous propagation in western (SING), eastern (I39PW and I40PG) and to a certain degree probably even northeastern directions (I30JP).

https://doi.org/10.5194/nhess-2019-179
Preprint. Discussion started: 11 June 2019

Natural Hazards and Earth System Sciences
Open Access
Discussions

The given attenuation modeling provides a map-based estimation where stratospheric conditions are favorable or unfavorable for infrasound ducting. Complementary to this, range-dependent propagation modeling is conducted between the epicenter and the four signal-detecting IMS arrays to estimate the loss of signal amplitude due to atmospheric attenuation as well as geometric spreading over the considerably large propagation distances of 1800 to 4500 km. This is performed to estimate if stratospheric propagation is possible, even under weak ducting conditions or conditions changing with distance.

Figure 4 shows the atmospheric ducting conditions and corresponding infrasound propagation for the four stations. For I39PW, I07AU and I40PG, stratospheric ducting is modeled in good agreement with the observed mean celerities of 290, 304 and 309 m/s (see table 1). Following *Negraru et al. (2010),* celerities for stratospheric ducting are expected to be in the order of 280 m/s to 320 m/s. Corresponding ray-tracing calculations (not shown here) estimate the celerities of those stratospheric ducts to be in the order of 290 m/s.

For I30JP, stratospheric ducting ceases along the 4500 km propagation path due to more unstable ducting conditions and higher transmission loss (about 150 dB). This is also in good agreement with the observations, since only a low-frequency signal is recorded at I30JP with a low celerity value of 263 m/s (ray-tracing suggesting 244 m/s), indicative not of a stratospheric but of a thermospheric arrival.

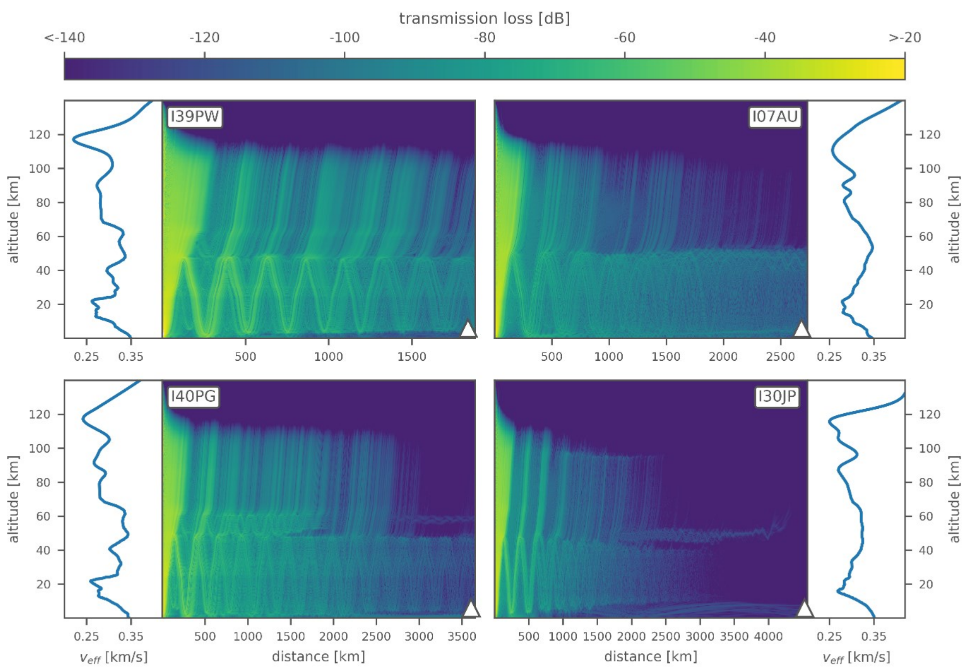

Fig 4: Propagation modeling between the Sulawesi earthquake epicenter (plot origins at 0 km distance) and the infrasound arrays I39PW, I07AU, I40PG and I30JP (respective triangles) using a range-dependent parabolic equation method, quantifying the transmission loss by atmospheric attenuation in dB relative to 1 km for a frequency of 1 Hz. Corresponding effective sound speed profiles (v_{eff}) are averaged over the complete propagation path.

Thermospheric ducts do not show up in figure 4, since this figure represents a 1 Hz modeling case highlighting the medium and high frequency stratospheric ducting and resulting in stronger absorption of thermospheric effects. For lower frequencies in the order of 0.01 Hz to 0.1 Hz, thermospheric attenuation is considerably small (*Sutherland and Bass, 2004)* and acoustic signal energy can propagate in the thermospheric duct over large distances with limited transmission loss.

The stability of the ducting conditions are best expressed by quantifying the effective sound speed (v_{eff}) ratio between the stratospheric maximum (at 40-60 km) and the ground along the propagation path. This parameter indicates favorable ducting conditions, when being equal or larger than 1 and unfavorable conditions otherwise. Nevertheless, *Le Pichon et al., 2012* and *Landès et al, 2014* point out that also v_{eff} ratios above 0.9 along the complete propagation path may lead to at least partially refracted energy in the stratosphere; whereas this ducting becomes highly likely for values above 0.95. While classical ray-trace modeling makes a strict separation between ratios larger or smaller than 1 (leading to existing or non-existing stratospheric ducts), the parabolic equation modeling used here also takes into account partial refractions of acoustic energy at effective sound speed ratios near but below 1. This is also a good representation of small-scale structures like atmospheric gravity waves varying atmospheric temperature and winds and thus also influencing the infrasound propagation (*Kulichkov et al., 2010; Green et al., 2011*).

The v_{eff} ratios of the average profiles depicted in figure 4 are 0.96 (I39PW), 1.00 (I07AU), 0.99 (I40PG) and 0.93 (I30JP), fully supporting the reasoning above. Not shown in figure 4 are the propagation cases to I06AU and I04AU, having no observations of the event and accordingly low v_{eff} ratios of 0.92 and 0.93, while the propagation to the single element station SING is indicative of stratospheric ducting with a higher v_{eff} ratio of 0.98.

5. Discussion and Conclusions

The main focus of the discussion of observed and modeled signals from the 28th September 2018 Sulawesi earthquake is on the source region and source mechanisms responsible for it. To support this discussion, a back-tracking procedure (comparable to the one applied in *Shani-Kadmiel et al., 2017* and in the supplement to *Gaebler et al., 2019*) is applied using the observed PMCC pixels and backtracking them using their temporal and directional information.

Figure 5 shows the back-projection results towards the island of Sulawesi in terms of an event density map of the pixel-by-pixel information on their most likely origin locations. A total number of about 107,000 pixels is used to derive the picture. Seismic speeds of 4 km/s, resembling the primary propagation of crustal seismic waves, are combined with 0.3 km/s acoustic celerities representing an average value of the station observations. The uncertainties of the measurements as well as the choice of a fixed seismic speed and acoustic celerity for all pixels instead of individual values is supposed to introduce an uncertainty to the back-projected locations as seen by the extended contour regions in figure 5. The velocity-averaged back-projection nevertheless sufficiently emphasizes the major source regions and infrasound generation mechanisms.

A region to the south of the epicenter is highlighted (yellow colors representing the highest event density), well corresponding with the earthquake rupture zone along the Palu-Koro fault line. Up to a certain degree, this method also serves as a cross-bearing location procedure, although stations contributing to it are not equally weighted but weighted by the number of pixels used from the respective stations (in this picture, I07AU dominates the back-projection, since it has the longest and largest record of the event); The location of the highest event density is at 119.6° E, 1.0° S, approximately 80 km south of the epicenter and thus half-way along the rupture.

https://doi.org/10.5194/nhess-2019-179
Preprint. Discussion started: 11 June 2019

Natural Hazards and Earth System Sciences
Open Access
EGU
Discussions

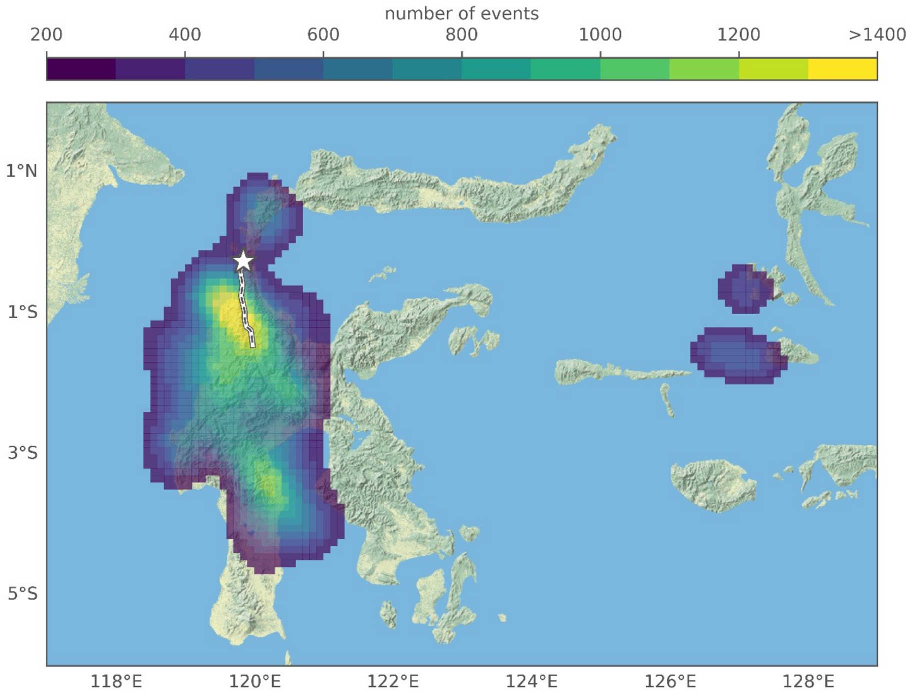

Fig 5: Back projection of the combined PMCC detections from I39PW, I07AU, I40PG and I30JP. Considered is each PMCC pixel's back-azimuth as well as a combination of 4 km/s seismic and 0.3 km/s acoustic celerities, resulting in seismoacoustic conversion locations. Color-coded event density for these locations is shown on a 0.1° x 0.1° grid, highlighting regions with more than 200 back-projected pixels per grid node. The epicenter is marked by an asterisk, the rupture zone traced by a dashed line.

The figure highlights that infrasound is radiated not only from a distinct, epicentral point source alone, but from a region extended in north-south directions following the rupture (in fact the event density values at the epicenter itself are lower than those in the surrounding regions). Secondary peaks apart from the basin region around the rupture are identified north of the epicenter and in the southern part of Sulawesi island. The pixels of this southern secondary color peak are mostly related to the early parts of the main signal recorded at I07AU, while the central and northern color peaks in the figure are related to signals arriving some minutes later. This corresponds to the 316° to 323° sweep in I07AU data from south to north, as described in section 3. The two side-maxima separated from the main signal's colored region are related to the secondary, seismoacoustic signatures described in section 3. They are derived from a number of I40PG PMCC pixels and point to a region near the North Maluku islands east of Sulawesi. Other secondary maxima as e.g. the ones between Java and east Timor, also mentioned in section 3, are beyond the map borders and not shown here.

In general, the results observed and visualized by figure 5 point out that an enlarged region, closely following the rupture and thus also the topography along the fault, generates the acoustic signals recorded at the remote infrasound sensors. This includes the rupture region itself suffering most from the earthquake-related ground movement (offsets of up to 7 m horizontal and 2 m dip slip) as well as an extended basin area around the rupture, enclosed by mountain chains in mostly north-to-south directions. Mountainous areas are a well-known source of secondary infrasound and seismoacoustic

https://doi.org/10.5194/nhess-2019-179
Preprint. Discussion started: 11 June 2019

signatures (e.g. *Arrowsmith et al., 2010*), and correspond to the event density maxima in figure 5: the mountain chains west and east of the Palu-Koro fault as well as the mountain area in the south of the island with the highest mountains of the Sulawesi island (Mt. Rantemario and Mt. Rantekombola, both about 3500 m elevation) generate large portions of the recorded signals. The less prominent but recognizable regions north of the epicenter (Mt. Fuyul Sojol, 3000 m elevation) and on the Maluku islands (e.g. Mt. Buku Sibela, 2000 m elevation) are also related to topographic peaks. The most likely source mechanism for the generation of large parts of the infrasonic and seismoacoustic signals is therefore estimated to be the shaking of elevated or exposed topography near the rupture zone, stimulated by crustal seismic or surface waves reaching these areas and turning them into motion.

To qualitatively assess if the super shear nature of the given earthquake or the regional prerequisites (or both) are responsible for the intense and long-lasting infrasound signals observed, the 28th September 2018 Sulawesi earthquake is compared to three other super shear earthquakes as well as three other normal shear earthquakes from the same region (Indonesia and Papua New Guinea). Shallow events between 5 - 30 km depth were chosen with comparably strong magnitudes of Mw >6.5 so that infrasound generation and detection can be expected. Table 2 chronologically lists these six events and provides an estimation of the emitted and observed infrasound for all of them.

Table 2: List of events similar to the 28th September 2018 Sulawesi earthquake, either in their super shear nature or in their regional origin. The "detecting IMS stations" (not necessary a complete list) as well the "source type / signal evaluation" are estimations following data analyses performed by authors of this study.

Event	Detecting IMS stations	Source type / signal evaluation
Denali, Alaska/USA, 03.11.2002, Mw 7.9, depth 4.9 km	I53US, I10CA	**Super shear earthquake,** short duration (10 minutes), strong infrasound at I53US (nearby), weak infrasound at I10CA (remote) generated by topography, also seismic arrivals
Sumatra Andaman, Indonesia, 26.12.2004, Mw 9.3, depth 30 km	I52GB, (others)	**Same region, normal shear earthquake,** long duration (30 minutes), strong infrasound, also seismic arrivals and secondary sources related to tsunami and tsunami-shoreline interaction
Quinghai, China, 13.04.2010, Mw 6.9, depth 17 km	I34MN	**Super shear earthquake,** short duration (<10 minutes), weak infrasound, no signal at stations in Japan or Russia, no seismic arrivals
Craig, Alaska/USA, 05.01.2013, Mw 7.5, depth 10 km	I53US, (I56US)	**Super shear earthquake,** short duration (<10 minutes), weak infrasound, I56US signals probably from other source, also seismic arrivals
Porgera, Papua New Guinea, 25.02.2018, Mw 7.5, depth 25.2 km	I06AU, I07AU, I39PW, I40PG	**Same region, normal shear earthquake,** long duration (20-60 minutes), strong infrasound related to nearby topography, also seismic arrivals
Kokopo, Papua New Guinea, 14.05.2019, Mw 7.5, depth 10 km	I22FR, I39PW, I40PG	**Same region, normal shear earthquake,** long duration (10-60 minutes), strong infrasound related to nearby topography, also seismic arrivals

https://doi.org/10.5194/nhess-2019-179
Preprint. Discussion started: 11 June 2019

The three super shear earthquakes named after Mount Denali, the Quinghai province and the city of Craig, occurring in 2002, 2010 and 2013, are the earthquakes most recent, most intense and most similar in their super shear characteristics to the 28th September 2018 Sulawesi earthquake, also having super shear rupture velocities of 4 to 6 km/s (see *Dunham and Archuleta, 2004; Wang and Mori, 2012*; *Yue et al., 2013*). Although the IMS infrasound network is not fully established yet (to the time of the Sulawesi earthquake, 80% of the stations were certified and operational, while it were only 8% to the time of the Denali earthquake and about 70% during the time of the other two earthquakes), at least one infrasound array was able to unambiguously detect and characterize each of the mentioned earthquakes.

The infrasound signals for Denali earthquake indicate strong infrasound signals at the nearby I53US station as well as much weaker signals at I10CA in a much larger distance. This event was a good opportunity to track the infrasound back to its generation region in the Alaska Mountain Range along the Denali fault where the rupture occurred (observed in I53US data, *Olsen et al., 2003*) and to the Rocky Mountain Chain south-east of it (observed in I10CA data). The strong movement of local and remote topography generated the infrasound in good agreement with the Sulawesi case. However, no indication is given that the super shear characteristics of the Denali earthquake specially favors the generation of infrasound. For the Quinghai and Craig earthquakes, also reported to be super shear, much weaker and shorter duration infrasound is observed at stations in distances of 400 km (I53US to Craig) to 1800 km (I34MN), compared to Sulawesi where stronger and much longer infrasound signals were observed between 1800 km and 4500 km. Again, these do not indicate any connection between those previous super shear earthquakes and extraordinary infrasound generation.

The Sulawesi earthquake is also compared to three strong earthquakes within the same region, most prominently two nearby Papua New Guinea earthquakes (near the Porgera mine, 2018 and Kokopo city, 2019) of the same magnitude occurring half a year before and after the Sulawesi one, showing strong and clearly observed infrasound signals at multiple IMS stations as well. These infrasound signals are observed up to similar distances as in the Sulawesi case and also provide long-duration, strong amplitude wave energy associated to infrasonic and seismoacoustic arrivals coming from the two earthquakes. Clear seismic signals are also present in the recordings (as in most cases described before, apart from Quinghai) and an association to topographic features as infrasound source regions is possible (the mountain chain in central Papua New Guinea for Porgera and the mountain areas in New Britain and New Ireland for Kokopo). For the Sumatra Andaman earthquake of 2004, strong infrasound with long signal durations was observed and could be back-tracked to topographic features of islands and shorelines, especially where the follow-up tsunami reached the shoreline of the Bay of Bengal (see *Le Pichon et al., 2005*). None of the presented earthquakes were super shear earthquakes, but all of them, especially the two very similar Papua New Guinea earthquakes generated strong infrasonic signals comparable to the signals of the Sulawesi event.

This leads to the conclusion that from comparison with other events, not the super shear nature of an earthquake is the most prominent or even exclusive feature linked to strong infrasound generated by an earthquake, but most likely the nearby existence of mountainous topography. This topography serves as a large-area resonating membrane in terms of large masses brought into motion by a triggering earthquake, which then produces large amounts of acoustic energy recorded at nearby or remote infrasound stations.

Since the given super shear event resembles one of only few large magnitude, shallow earthquakes generating pronounced infrasound, it provides a unique opportunity to study earthquake generated infrasound in terms of the source mechanisms, signal characteristics, propagation conditions and ducting behavior. It also supports the improved understanding of the process of stimulating infrasound radiation by mountain shaking from large earthquakes and the conversion of seismic to acoustic energy.

While this study provides the observation analyses and modeling results for the Sulawesi earthquake and a qualitative comparison to other events, it cannot provide a comprehensive investigation taking into account every detail to upmost precision. Measurement uncertainties are due to the instrumentation and methods applied; modeling uncertainties are due to assumptions applied within the models and due to multi-scale atmospheric variations between source and receivers leading to uncertainties in the attenuation and propagation calculations. Taking into account these uncertainties and improving the methods and models to cope with them in the future will help to gain novel and enhanced insights about infrasound observations and modeling in general and earthquake generated infrasound in particular. This will also help to optimize seismoacoustic observation networks in terms of better understanding the instrumental needs and better evaluating the signatures observable by it. It will finally support seismoacoustic studies of natural as well as anthropogenic infrasound sources in the future and thereby support the infrasound monitoring for treaty verification purposes of the CTBT.

Acknowledgements

This work comprises Earth Observatory of Singapore contribution no. XXX.

Data availability

Information about earthquake magnitude, location and frequency of occurrence in the region of interest is retrieved from the online-accessible archive of the USGS, see https://earthquake.usgs.gov/earthquakes/ (last accessed 23.05.2019).

Atmospheric wind and temperature profiles are derived from the ECMWF, available at https://www.ecmwf.int/ (last accessed 23.05.2019).

Waveform data for the infrasound arrays of the CTBTO IMS (https://www.ctbto.org/) used in this study are available to the authors being members of National Data Centers for the CTBTO. Waveform data for SING infrasound station are available to the authors being members of the Earth Observatory of Singapore.

Competing Interests

none

Author Contributions

CP analyzed the waveform data, performed the propagation modeling, wrote the manuscript text and coordinated the co-author contributions; **PG** compiled the data, generated the figures and helped with finalizing the manuscript layout; **LC** provided first ideas and initiated the collaborative study; **ALP** provided expertise in earthquake infrasound, comparison to other events and initiated the collaborative study; **JV** analyzed the waveform data and performed propagation modeling; **AP** analyzed the waveform data and provided manuscript text; **DT** performed the attenuation modeling

https://doi.org/10.5194/nhess-2019-179
Preprint. Discussion started: 11 June 2019

Natural Hazards and Earth System Sciences
Discussions

and provided manuscript text; **BT** provided first ideas and initiated the collaborative study; **all authors** supported and improved the draft by proof-reading, commenting or correcting the manuscript.

References

Arrowsmith, S.J., Johnson, J.B., Drob, D.P., and Hedlin, M.A.H.: The seismoacoustic wavefield: A new paradigm in studying geophysical phenomena, Review of Geophysics, 48, doi: 10.1029/2010RG000335, 2010.

Bao, H., Ampuero, J.-P., Meng, L., Fielding, E.J., Liang, C., Milliner, C.W.D., Feng, T., and Huang, H.: Early and persistent supershear rupture of the 2018 magnitude 7.5 Palu earthquake, Nature Geoscience, 12, doi: 10.1038/s41561-018-0297-z, 2019.

Bouchon, M., Toksöz, N., Karabulut, H., Bouin, M.-P., Dietrich, M., Aktar, M., and Edie, M.: Seismic imaging of the 1999 Izmit (Turkey) Rupture inferred from the near-fault recordings, Geophysical Research Letters, 27, doi: 10.1029/2000GL011761, 2000.

Bouchon, M. and Vallée, M.: Observation of Long Supershear Rupture during the Magnitude 8.1 Kunlunshan Earthquake, Science, 301, doi: 10.1126/science.1086832, 2003.

Cansi, Y.: An automatic seismic event processing for detection and location: the PMCC method, Geophysical Research Letters, 22, doi: 10.1029/95GL00468, 1995.

Drob, D. P., Picone, J. M., and Garcés, M. A.: Global morphology of infrasound propagation, Journal of Geophysical Research, 108, doi: 10.1029/2002JD003307, 2003.

Drob, D. P., Emmert, J. T., Crowley, G., Picone, J. M., Shepherd, G. G., Skinner, W., Hays, P., Niciejewski, R. J., Larsen, M., She, C. Y., Meriwether, J. W., Hernandez, G., Jarvis, M. J., Sipler, D. P., Tepley, C. A., O'Brien, M. S., Bowman, J. R., Wu, Q., Murayama, Y., Kawamura, S., Reid, I. M., and Vincent R. A.: An Empirical Model of the Earth's Horizontal Wind Fields: HWM07, Journal of Geophysical Research, 113, doi: 10.1029/2008JA013668, 2008.

Dunham, E.M. and Archuleta, R. J.: Evidence for a Supershear Transient during the 2002 Denali Fault Earthquake, Bulletin of the Seismological Society of America, 94, doi: 10.1785/0120040616, 2004.

Gaebler, P., Ceranna, L., Nooshiri, N., Barth, A., Cesca, S., Frei, M., Grünberg, I., Hartmann, G., Koch, K., Pilger, C., Ross, J. O., and Dahm, T.: A multi-technology analysis of the 2017 North Korean nuclear test, Solid Earth, 10, doi: 10.5194/se-10-59-2019, 2019.

Garcés, M. A.: On Infrasound Standards, Part 1: Time, Frequency, and Energy Scaling, InfraMatics 2, doi: 10.4236/inframatics.2013.22002, 2013.

Gibbons, S. J., Asming, V., Eliasson, L., Fedorov, A., Fyen, J., Kero, J., Kozlovskaya, E., Kvaerna, T., Liszka, L., Näsholm, S. P., Raita, T., Roth, M., Tiira, T., and Vinogradov, Y.: The European Arctic: A Laboratory for Seismoacoustic Studies, Seismological Research Letters, 86, doi: 10.1785/0220140230, 2015a.

Gibbons, S. J., Kværna, T., and Mykkeltveit, S.: Could the IMS Infrasound Stations Support a Global Network of Small Aperture Seismic Arrays?, Seismological Research Letters, 86, doi: 10.1785/0220150068, 2015b.

Green, D.N., Vergoz, J., Gibson, R., Le Pichon A., and Ceranna, L.: Infrasound radiated by the Gerdec and Chelopechene explosions: propagation along unexpected paths, Geophysical Journal International, 185, doi: 10.1111/j.1365-246X.2011.04975.x, 2011.

Hedlin, M.A.H., Walker, K. T., Drob, D. P., and de Groot-Hedlin, C. D.: Infrasound: Connecting the Solid Earth, Oceans, and Atmosphere, Annual Review of Earth and Planetary Sciences, 40, doi: 10.1146/annurev-earth-042711-105508, 2012.

Heidarzadeh, M., Muhari, A., and Wijanarto, A.B.: Insights on the Source of the 28 September 2018 Sulawesi Tsunami, Indonesia Based on Spectral Analyses and Numerical Simulations, Pure and Applied Geophysics, 176, doi: 10.1007/s00024-018-2065-9, 2019.

Hernandez, B., Le Pichon, A., Vergoz, J., Herry, P., Ceranna, L., Pilger, C., Marchetti, E., Ripepe, M., and Bossu, R.: Estimating the Ground-Motion Distribution of the 2016 Mw 6.2 Amatrice, Italy, Earthquake Using Remote Infrasound Observations, Seismological Research Letters, 89, doi: 10.1785/0220180103, 2018.

Katili, J. A.: Past and Present Geotectonic Position of Sulawesi, Indonesia, Tectonophysics, 45, doi: 10.1016/0040-1951(78)90166-X, 1978.

Kulichkov, S.N., Chunchuzov, I. P., and Popov, O. I.: Simulating the Influence of an Atmospheric Fine Inhomogeneous Structure on Long Range Propagation of Pulsed Acoustic Signals, Izvestiya Atmospheric and Oceanic Physics, 46, doi: 10.1134/S0001433810010093, 2010.

Landès, M., Le Pichon, A., Shapiro, N.M., Hillers, G., and Campillo, M.: Explaining global patterns of microbarom observations with wave action models, Geophysical Journal International, 199, doi: 10.1093/gji/ggu324, 2014.

Le Pichon, A., Guilbert, J., Vega, A., Garcés, M. A., and Brachet, N.: Ground-coupled air waves and diffracted infrasound from the Arequipa earthquake of June 23, 2001, Geophysical Research Letters, 29, doi: 10.1029/2002GL015052, 2002.

Le Pichon, A., Guilbert, J., Vallée, M., Dessa, J. X., and Ulziibat, M.: Infrasonic imaging of the Kunlun Mountains for the great 2001 China earthquake, Geophysical Research Letters, 30, doi: 10.1029/2003GL017581, 2003.

Le Pichon, A., Herry, P., Mialle, P., Vergoz, J., Brachet, N., Garces, M. A., Drob, D., and Ceranna, L.: Infrasound associated with 2004-2005 large Sumatra earthquakes and tsunami, Geophysical Research Letters, 32, doi: 10.1029/2005GL023893, 2005.

Le Pichon, A., Mialle, P., Guilbert, J., and Vergoz, J.: Multistation infrasonic observations of the Chilean earthquake of 2005 June 13, Geophysical Journal International, 167, doi: 10.1111/j.1365-246X.2006.03190.x, 2006.

Le Pichon, A., Blanc, E., and Hauchecorne, A. (Eds.): Infrasound Monitoring for Atmospheric Studies, Springer, ISBN: 978-1-4020-9507-8, 2010.

Le Pichon, A., Ceranna, L., and Vergoz, J.: Incorporating numerical modeling into estimates of the detection capability of the IMS infrasound network, Journal of Geophysical Research, 117, doi: 10.1029/2011JD016670, 2012.

Le Pichon, A., Blanc, E., and Hauchecorne, A. (Eds.): Infrasound for Atmospheric Studies – Challenges in Middle Atmosphere Dynamics and Societal Benefits, Springer, ISBN: 978-3-319-75138-2, 2019.

Marchetti, E., Lacanna, G., Le Pichon, A., Piccinini, D., and Ripepe, M.: Evidence of large infrasonic radiation induced by earthquake interaction with alluvial sediments, Seismological Research Letters, 87, doi: 10.1785/0220150223, 2016.

https://doi.org/10.5194/nhess-2019-179
Preprint. Discussion started: 11 June 2019

Natural Hazards and Earth System Sciences
Open Access
Discussions

Mutschlecner, J. P. and Whitaker, R. W.: Infrasound from earthquakes, Journal of Geophysical Research, 110, doi: 10.1029/2004JD005067, 2005.

Negraru, P. T., Golden, P., and Herrin, E.T.: Infrasound Propagation in the "Zone of Silence", Seismological Research Letters, 81, doi: 10.1785/gssrl.81.4.615, 2010.

Olson, J.V., Wilson, C.R., and Hansen, R.A.: Infrasound associated with the 2002 Denali fault earthquake, Alaska, Geophysical Research Letters, doi: 10.1029/2003GL018568, 2003.

Omira, R., Dogan, G. G., Hidayat, R., Husrin, S., Prasetya, G., Annunziato, A., Proietti, C., Probst, P., Paparo, M. A., Wronna, M., Zaytsev, A., Pronin, P., Giniyatullin, A., Putra, P. S., Hartanto, D. , Ginanjar, G., Kongko, W., Pelinovsky, E., and Yalciner, A. C.: The September 28th, 2018, Tsunami In Palu-Sulawesi, Indonesia: A Post-Event Field Survey, Pure and Applied Geophysics 176, doi: 10.1007/s00024-019-02145-z, 2019.

Pailoplee, S.: Probabilities of Earthquake Occurrences along the Sumatra-Andaman Subduction Zone, Open Geosciences, 9, doi: 10.1515/geo-2017-0004, 2017.

Picone, J. M., Hedin, A. E., Drob, D. P., and Aikin, A. C.: NRLMSISE-00 Empirical Model of the Atmosphere: Statistical Comparisons and Scientific Issues, Journal of Geophysical Research, 107, doi: 10.1029/2002JA009430, 2002.

Pilger, C., Ceranna, L., Ross, J.O., Vergoz, J., Le Pichon, A., Brachet, N., Blanc, E., Kero, J., Liszka, L., Gibbons, S., Kvaerna, T., Näsholm, S.P., Marchetti, E., Ripepe, M., Smets, P., Evers, L., Ghica, D., Ionescu, C., Sindelarova, T., Ben Horin, Y., and P. Mialle: The European Infrasound Bulletin, Pure and Applied Geophysics, 175, doi: 10.1007/s00024-018-1900-3, 2018.

Shani-Kadmiel, S., Assink, J.D., Smets, P.S.M., and Evers, L.G.: Seismoacoustic coupled signals from earthquakes in Central Italy: epicentral and secondary sources of infrasound, Geophysical Research Letters, 45, doi: 10.1002/2017GL076125, 2017.

Socquet, A., Hollingsworth, J., Pathier, E., and Bouchon, M.: Evidence of supershear during the 2018 magnitude 7.5 Palu earthquake from space geodesy, Nature Geosciences, 12, doi: 10.1038/s41561-018-0296-0, 2019.

Sutherland, L. C. and Bass, H. E.: Atmospheric absorption in the atmosphere up to 160 km, Journal of the Acoustical Society of America, 115, doi: 10.1121/1.1631937, 2004.

Tailpied, D., Le Pichon, A., Marchetti, E., Assink, J., and Vergniolle, S.: Assessing and optimizing the performance of infrasound networks infrasound networks to monitor volcanic eruptions, Geophysical Journal International, 208, doi: 10.1093/gji/ggw400, 2017.

Wang, D. and Mori, J.: The 2010 Qinghai, China, Earthquake: A Moderate Earthquake with Supershear Rupture, Bulletin of the Seismological Society of America, 102, doi: 10.1785/0120110034, 2012.

Waxler, R., Assink, J., Hetzer, C., and Velea, D.: NCPAprop – A software package for infrasound propagation modeling, Journal of the Acoustical Society of America, 141, doi: 10.1121/1.4987797, 2017.

Wilson, D. K.: The sound-speed gradient and refraction in the near-ground atmosphere, Journal of the Acoustical Society of America, 113, doi: 10.1121/1.1532028, 2003.

Yue, H., Lay, T., Freymueller, J. T., Ding, K., Rivera, L., Ruppert, N. A., and Koper, K. D.: Supershear rupture of the 5 January 2013 Craig, Alaska (Mw 7.5) earthquake, Journal of Geophysical Research, doi: 10.1002/2013JB010594, 2013.